Estimation of in-vivo cerebrospinal fluid velocity using fMRI inflow effect

Tyler C. Diorio[1], Vidhya Vijayakrishnan Nair[1], Lauren E. Hedges[1], Vitaliy L. Rayz[1], Yunjie Tong[1]

[1]Weldon School of Biomedical Engineering, Purdue University, West Lafayette, IN

Abstract

In-vivo estimation of cerebrospinal fluid (CSF) velocity is crucial for understanding the glymphatic system and its potential role in neurodegenerative disorders such as Alzheimer's disease, Parkinson's disease, and multiple sclerosis. Current cardiac or respiratory gated approaches, such as 4D Flow MRI, cannot capture CSF movement in real time due to limited temporal resolution and in addition deteriorate in accuracy at low fluid velocities. Other techniques like real-time PC-MRI or time-spatial labeling inversion pulse are not limited by temporal averaging but have limited availability even in research settings. This study aims to quantify the inflow effect of dynamic CSF motion on functional magnetic resonance imaging (fMRI) for *in-vivo,* real-time measurement of CSF flow velocity. We considered linear and exponential models of velocity waveforms and empirically fit them to fMRI data from a controlled flow experiment. To assess the utility of this methodology in human data, CSF flow velocities were computed from fMRI data acquired in eight healthy volunteers. Breath holding regimens were used to amplify CSF flow oscillations. Our experimental flow study revealed that CSF velocity is exponentially related to inflow effect-mediated signal increase. Using this relationship, we recovered velocity from *in vivo* fMRI signal, demonstrating the potential of our approach for estimating CSF flow velocity in the human brain. This novel method could serve as an alternative approach to quantifying slow flow velocities in real time, such as CSF flow in the ventricular system, thereby providing valuable insights into the glymphatic system's function and its implications for neurological disorders.

Introduction

The recently proposed glymphatic system involves the interchange of cerebrospinal fluid (CSF) and interstitial fluid (ISF) within the perivascular space resulting in the elimination of waste from the central nervous system (CNS)[11,13]. The network of perivascular spaces surrounding blood vessels in the brain facilitates the clearance of metabolic waste products, such as beta-amyloid, from the brain[10]. This system is unique in that its function is elevated during sleep, when the brain is at rest[20]. The malfunctioning of the glymphatic system has been associated with the buildup of harmful proteins in the brain, potentially resulting in a decline in cognitive function and the degeneration of nerve cells. Recent studies have shown that the glymphatic system may play a role in the development and progression of neurological disorders such as Alzheimer's disease, Parkinson's disease, and multiple sclerosis[2,17,27].

As a result, attention has been turned to understanding the flow of CSF within the brain and how it is affected by cardiac, respiratory, and low frequency oscillations[4,18]. Previous work has shown that respiration is a major regulator of CSF flow, with physiological alterations by respiratory pattern driving changes in the magnitude and directionality of CSF flow[3,15,18,23]. Hypercapnia, or an increase in the level of carbon dioxide in the blood, can be induced through respiratory patterning, such as breath holding, and causes arterial vasodilation in the brain. As per the Monro-Kellie doctrine, changes in a volume component, such as arterial vasodilation, within the fixed volume of the skull causes compensatory changes in at least one other components, such as CSF outflow[16].

MRI flow measurements are often utilized as a non-invasive approach to visualize and quantify the macroscale flow of CSF. MRI flow imaging sequences, such as planar or three-directional (4D Flow) phase-contrast, can be used to detect CSF motion but are restricted within one cardiac/respiratory cycle due to gating constraints[24]. Only a few studies observe real-time CSF movement, using either real-time phase-contrast techniques[19,25] or time-spatial labeling inversion pulse[21,22]. Additionally, these sequences are often not available at research scanners since they are uncommon or new imaging sequences. Another imaging technique, blood oxygen level-dependent functional magnetic resonance imaging (BOLD fMRI) is sensitive to changes in the magnetic properties of blood as it flows through the brain[9]. In the context of CSF flow, BOLD fMRI can be used indirectly to detect real-time changes in the velocity of CSF flow through the brain ventricles and subarachnoid spaces by accounting for inflow effect-mediated signal increases.

Fultz et al. utilized BOLD fMRI ($TR < 400$ ms), to study the temporal patterning of electrophysiology, hemodynamics, and CSF movements[4]. Their study maximized inflow effect mediated signal increases by carefully placing the first slice of their imaging volume at the bottom of the fourth ventricle, where cranial-directed flow-mediated inflow effect would be greatest. Their work described a critical velocity value that is required to completely replace the CSF in a given voxel, however they did not delve into quantifying the underlying velocity.

Using a combination of flow physics, MR imaging experiments, and human CSF fMRI data, our present study seeks to further understand and quantify the inflow effect of dynamic CSF motion on fMRI for *in-vivo* measurement of real-time CSF flow velocity. Specifically, we assessed linear and exponential models of velocity predictions by empirically fitting to fMRI data from a controlled flow experiment. To assess the utility of this methodology in human data, we also computed velocities on CSF flow data from eight healthy volunteers, where breathing protocols were used to amplify CSF flow oscillations.

Methods

The inflow effect on fMRI

The inflow effect refers to the increase in MRI signal intensity that occurs when fresh fluid (not exposed to radiofrequency pulses) enters a region of the imaging volume, as demonstrated in **Figure 1** for various inflow scenarios. Each of the scenarios in **Figure 1** corresponds to a specific increase of the signal, which we seek to quantify. As fresh fluid moves into the imaging volume between RF pulses, it induces higher signal intensity via apparent T1 shortening. The inflow effect is distinct from the BOLD effect in origin, and its contribution to the fMRI signal can distort the hemodynamic response estimated in an event-related fMRI experiment[5]. The inflow effect is more significant when a short repetition time (TR) and large flip angle are used in a single-shot gradient-echo (GE) EPI sequence. The inflow contribution to the fMRI signal increases monotonically in spoiled gradient-echo sequences, while the fMRI signal may increase or decrease in conventional refocused gradient-echo sequences[5].

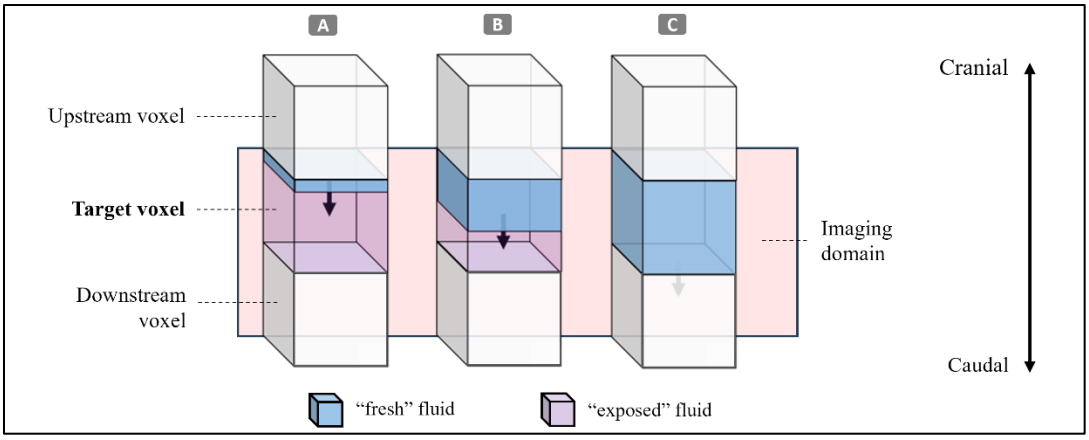

Figure 1: *Graphical representation of possible configurations of flow changes between temporal fMRI acquisitions, where blue shading represents fluid that was originally outside of the imaging domain (termed "fresh"), and purple represents fluid that was inside the imaging domain (termed "exposed") at the previous time step. The three stacks (A-C) represent minimal (A), majority (B), and full (C) amounts of "fresh" fluid flowing caudally from the upstream voxel.*

Given that each voxel holds a volume defined by the spatial resolution of the imaging domain, we theorize that the maximum possible signal increase occurs when the full volume of a given voxel has been "refreshed" with incoming fluid in each repetition time (TR), shown as Stack 1 and 6 in **Figure 1**. This would be accomplished by a voxel-average critical fluid velocity (v_{crit}), which is equal to the edge length (z) perpendicular to the fluid flow direction divided by the time frame of repetition (TR) for an fMRI EPI scan:

$$v_{crit} = \frac{z}{TR} \quad (1)$$

Assuming that v_{crit} corresponds to a maximum signal observed on fMRI, we can use a simple linear theoretical model to estimate instantaneous velocity, v(t) by scaling the normalized instantaneous fMRI signal (f(t)) by the critical velocity, as demonstrated below:

$$v(t) = v_{crit} * f(t) \quad (2)$$

Experimental flow study and fMRI

To test this linear model, we designed a controlled flow imaging study for a fixed set of parameters representative of the *in-vivo* imaging conditions. The flow loop, partially diagrammed in Figure 2A-B, involved a programmable syringe flow pump (Legato 210, KD Scientific) loaded with a 100mL syringe fitted via Luer lock to a 4-mm inner diameter length of tubing, connected to a 10-mm inner diameter tube which was passed through the MRI Scanner (GE 3-T) and Head Coil (64-Channel, GE) then submerged into a fluid reservoir outlet.

The fMRI scans were acquired by using a multiband echo-planar imaging (EPI) sequence (FOV = 120 mm, acquisition matrix =64 x 64, 10 slices, voxel size = $2.9 \times 2.9 \times 2.9\ mm^3$, TR/TE = 440/20.3 ms, echo-spacing = 0.644 ms, flip angle = 35°, hyperband acceleration factor = 8, multi-slice mode: interleaved). The imaging volume was placed perpendicular to the flow direction in the head coil (**Figure 2C**), with the target voxels set on the first slice of voxels exposed to flow in the head coil, where inflow effect-mediated signal increase is greatest.

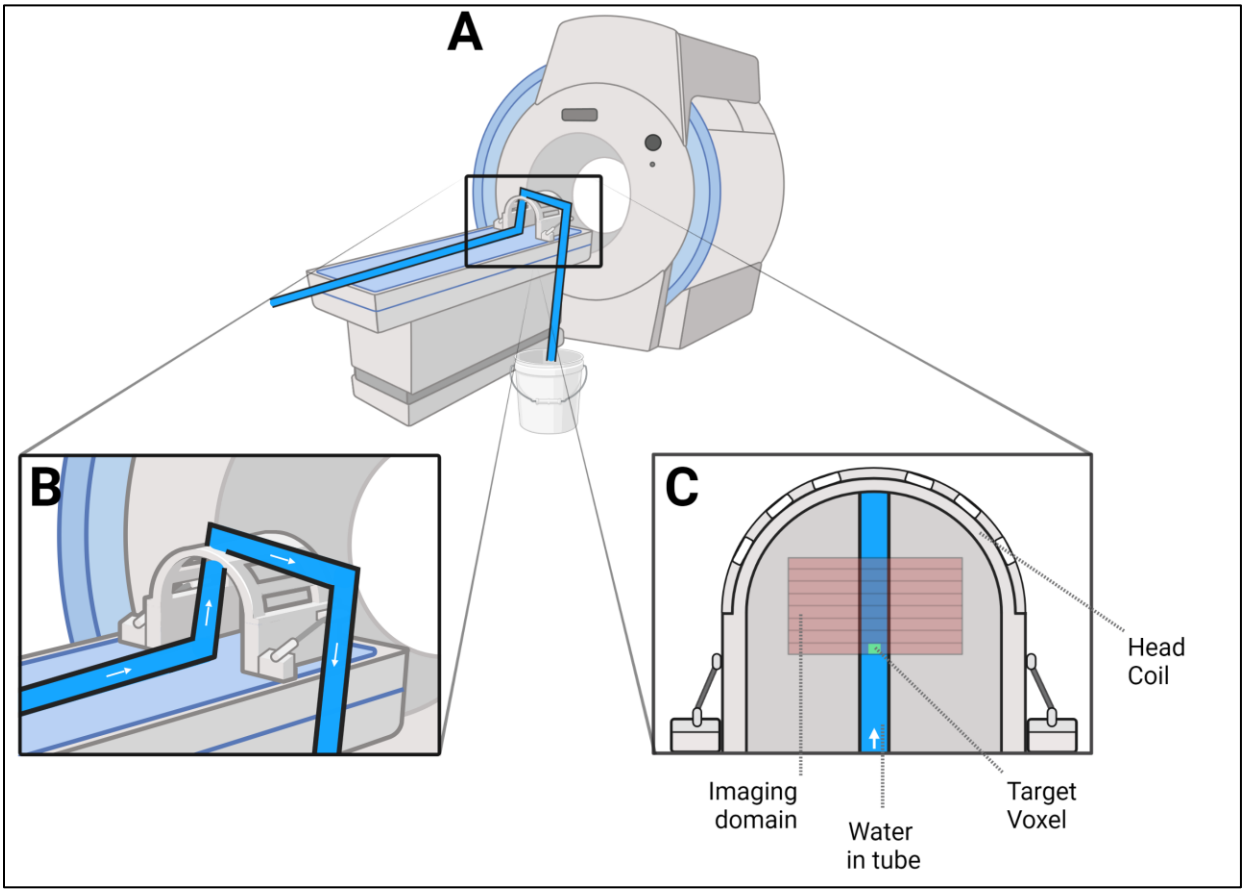

***Figure 2**: **(A)** Graphical representation of experimental flow loop and MRI scanning room set-up. **(B)** Expanded view of the flow and tube orientation within the 64-channel head coil, where blue fluid represents water and white arrow denotes steady flow direction. **(C)** Diagram view of the MRI slice selection within the head coil where the target voxel (denoted by a green square) is placed at the bottom of the imaging volume. Image created in BioRender.*

The v_{crit} for these experimental flow studies, given the isotropic spatial resolution of 2.9 mm and TR of 440 ms, was computed to be 6.59 mm/s. Thus, ten equally spaced inflow velocities, spanning 1 mm/s to 10 mm/s, were repeated over 3 trials to provide a range of velocities above and below the critical velocity within the 10-mm tube. Given the fixed 100mL volume of the syringe, rest intervals between velocity conditions allowed us to reset the syringe pump and fluid volumes.

Experimental data processing

Measured fMRI signals for each of the three trials were analyzed by first selecting four target voxels which are aligned perpendicular to flow and in the same z-slice of the imaging volume (**Figure 3A**) to obtain a better spatial average of the flow temporal waveform. The fMRI signal was normalized for each voxel by subtracting 10^{th} percentile minimum lower bounds from the raw fMRI signal, dividing by the 95^{th} percentile maximum upper bounds, and thresholding from 0 to 1 to reduce noise. Then, the normalized target voxels were spatially averaged within each trial to better approximate the mean velocity within the tube, with standard deviation quantified across target voxels within trial (**Figure 3B**). Qualitative observation showed increased noise in trials 2 and 3 likely due to air bubbles in the flow loop, thus data from trial 1 has been used to visualize the results of this study.

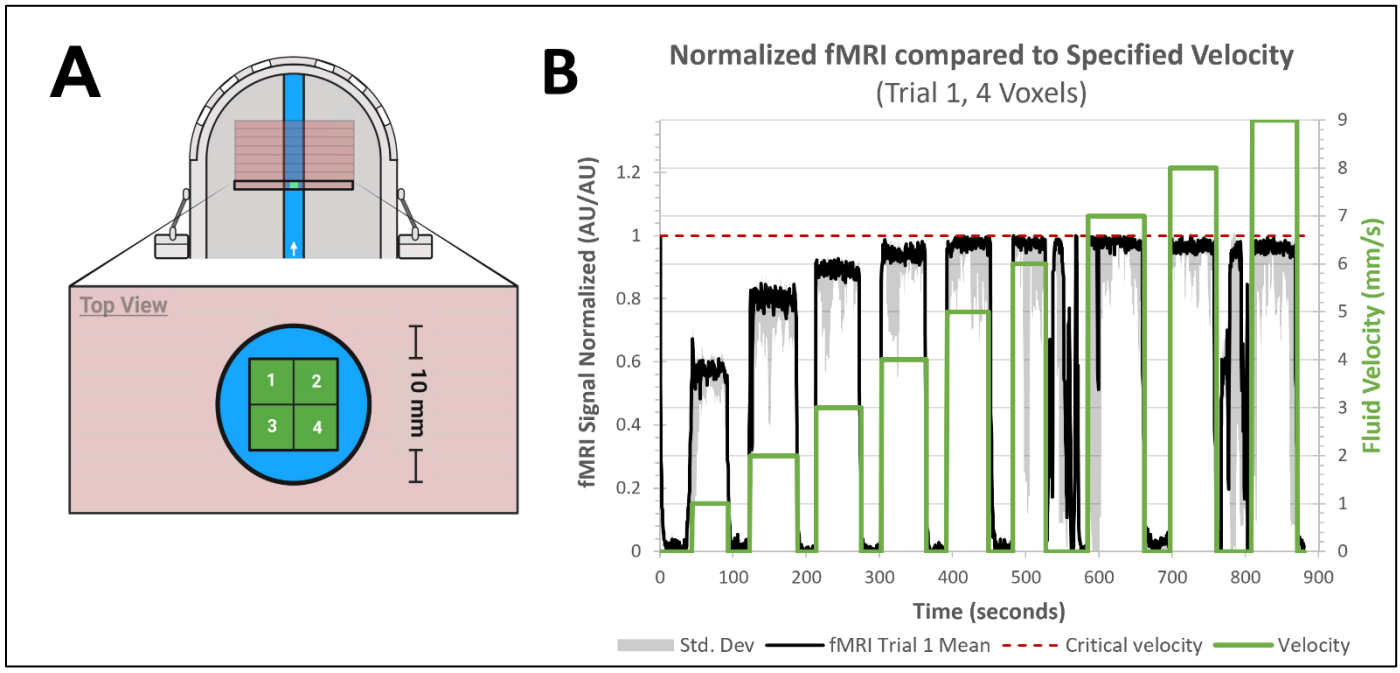

***Figure 3**: **(A)** Diagram of spatial averaging across 4 voxels center to the flow within the first slice of the imaging volume oriented perpendicular to flow. **(B)** Data comparison of temporal profiles at 1 voxel (30 30 0) between estimated fluid velocity (green) as set via the syringe pump and measured, normalized fMRI signal (black), where the red dashed line denotes the critical velocity at which is the target voxel would be fully refreshed with new fluid in each TR. Signal oscillations occurring between 500-600 second time points are a result of exchanging syringe volumes and resetting the syringe pump due to volume considerations*

Linear and exponential fits were constructed using the *`fit()`* function in MATLAB (MathWorks, R2021a) by specifying the mean measured fMRI signal, f(t), as x-data and the specified velocity, v(t), as the y-data (**Figure 4A**). Linear fitting was conducted simply by specifying a single constant linear model where the constant is defined to be the critical velocity, as calculated according to the equation (2). Exponential fitting was conducted by specifying a two-constant exponential model where one constant was defined to be the critical velocity and the other was fit to the data:

$$v(t) = a * e^{v_{crit} * f(t)} \quad (3)$$

In-vivo structural and functional MRI scans

To test the exponential relation of fMRI signal to velocity using the inflow effect, we recruited healthy volunteers (n=8) aged 19 – 48 (25.75 ± 9.53) years to undergo a series of structural and fMRI scans that included both resting state and breath holding regimens. Structural T1-weighted MPRAGE (Magnetization Prepared Rapid Acquisition Gradient Echo - TR/TE: 2300/2.26 ms, 192 slices per slab, flip angle: 8°, resolution: 1.0mm × 1.0mm × 1.0mm) images were acquired first to accurately locate the fourth ventricle, followed by the functional scans. For the resting state scans, the volunteers were instructed via visual cues to breathe normally. For the breath holding scans, the volunteers were instructed to breathe normally (15-seconds), followed by paced breathing (18 seconds - three repeats of a 3-second inhale and 3-second exhale), and then breath hold (20 seconds) at for a total of 6 cycles. s. The fMRI scans were acquired by using a multiband EPI sequence (FOV = 230 mm, acquisition matrix =92 × 92, 48 slices, voxel size = 2.5 × 2.5 × 2.5 mm^3, TR/TE = 440/30.6 ms, echo-spacing = 0.51 ms, flip angle = 35°, hyperband acceleration factor = 8, multi-slice mode: interleaved) on a 3T SIEMENS Scanner at Purdue MRI Facility. The imaging volumes were placed perpendicular to the fourth ventricle with the edge of the volume at the bottom of the fourth ventricle and extending caudal into the neck as described in Figure 3 of Nair et al. 2022. Target voxels were set on the upper most (cranial) slice, where inflow effect-mediated signal increase is greatest, to understand outflow from the brain to the neck in the ventricular system.

In-vivo data processing

fMRI scans were preprocessed using FSL [FMRIB Expert Analysis Tool, v6.01; Oxford University, United Kingdom][12] and MATLAB (MATLAB 2020b; The MathWorks Inc., Natick, MA, 2000). As described previously[4,18,24], preprocessing steps only included slice timing correction and registration with the structural T1-Weighted image, before extracting the fMRI inflow signal from a target voxel at the center of the fourth ventricle. Measured fMRI signals for each of the resting state and breath holding scans were analyzed by first applying detrending on the target voxel within each subject to match protocols from human data and address signal drift using the MATLAB *`detrend()`* function. The detrended fMRI signal was normalized for each voxel by subtracting 10th percentile minimum lower bounds from the raw fMRI signal, dividing by the 95th percentile maximum upper bounds, and thresholding from 0 to 1 to reduce noise. The upper and lower bounds were searched within subjects, due to inter-subject variability, and across breathing patterns, as large CSF flow velocities can occur either during resting state or breath holding. Then, the normalized signals were reconstructed into temporal velocity waveforms using the exponential and linear fits from the experimental study.

Results

Flow speed is exponentially related to inflow effect-mediated signal increase

Using an experimental flow loop and multiband EPI fMRI sequence, we quantified the relationship between measured fMRI signal increase due to the inflow effect and estimates of the underlying velocity of fluid, as shown in **Figure 3B**. The measured fMRI signal increase due to inflow effect related non-linearly to the underlying velocity. An exponential fit was found to reasonably estimate the underlying velocity in our experimental data (**Figure 4A**).

To qualitatively understand the impact of differences in recovering velocities using the linear and exponential fits, we calculated the temporal velocity waveform using the measured fMRI signals (**Figure 4B**). It can be observed that the linear model (red) is insufficient for reconstructing velocities below the critical velocity, whereas the exponential model (blue) provides a closer approximation at all levels below the critical velocity. It is important to note that neither model can resolve velocities above the critical velocity due to the notion that signal is proportional to unexposed fluid which is maximally refreshed at flow speeds equal to or above the critical velocity.

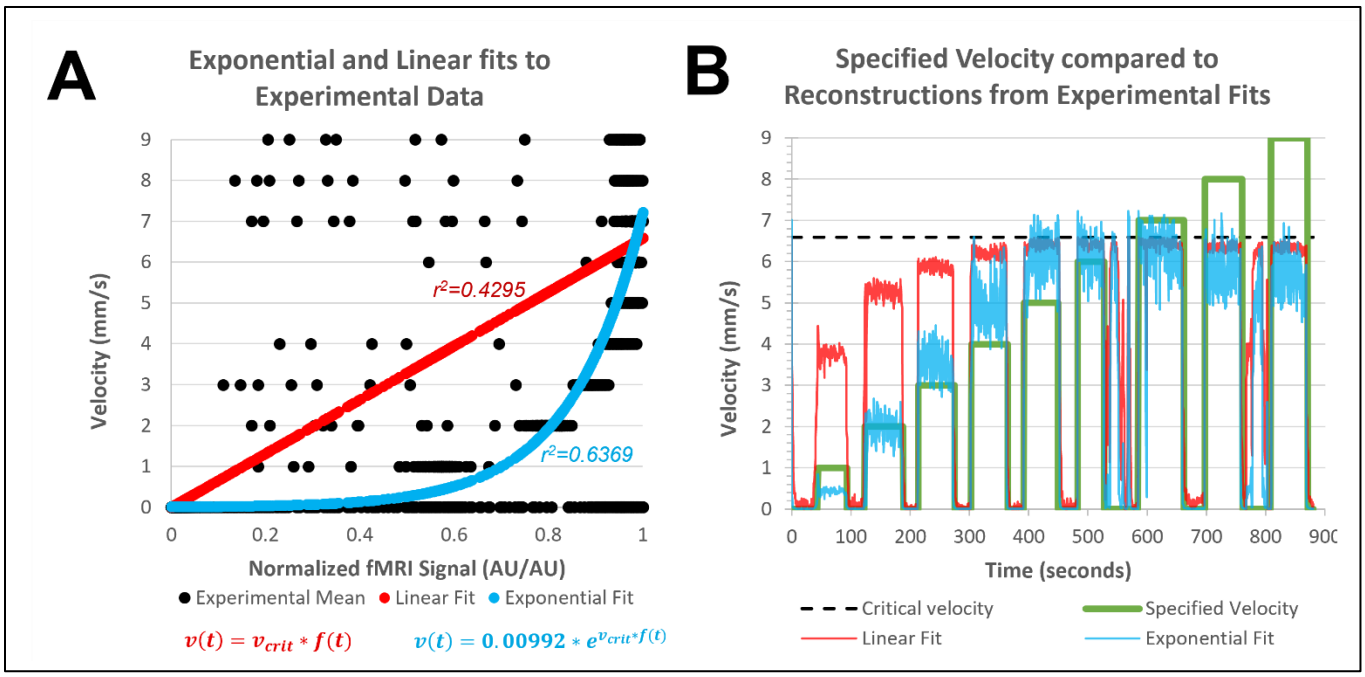

Figure 4: ***(A)*** *Linear (red) and exponential (blue) fits for the experimentally specified velocity data (black), demonstrating R^2 values of 0.4295 and 0.6369 for the linear and exponential fits, respectively.* ***(B)*** *Using the linear (red) and exponential (blue) fits from (A), measured fMRI data was reconstructed to compare against the specified velocity data (green). Critical velocity is shown as a dashed black line.*

Velocity recovered from in vivo fMRI signal

The exponential and linear models were also applied to the *in vivo* data to visually demonstrate their ability to estimate underlying velocities, from which a representative subject case as well as a group average (n=8) as shown in **Figure 5**. The exponential model reduces the impact of lower fMRI signal increases on reconstructed velocities as well as sharpens the temporal changes in velocity, as shown in **Figure 5C**. Both reconstructed velocity waveforms span a range from zero to the critical velocity of the *in vivo* scans. Notably, the signal and velocity waveforms follow a distinctly cyclical pattern in the breath holding data which highlights the utility of using breathing challenges to alter CSF motion.

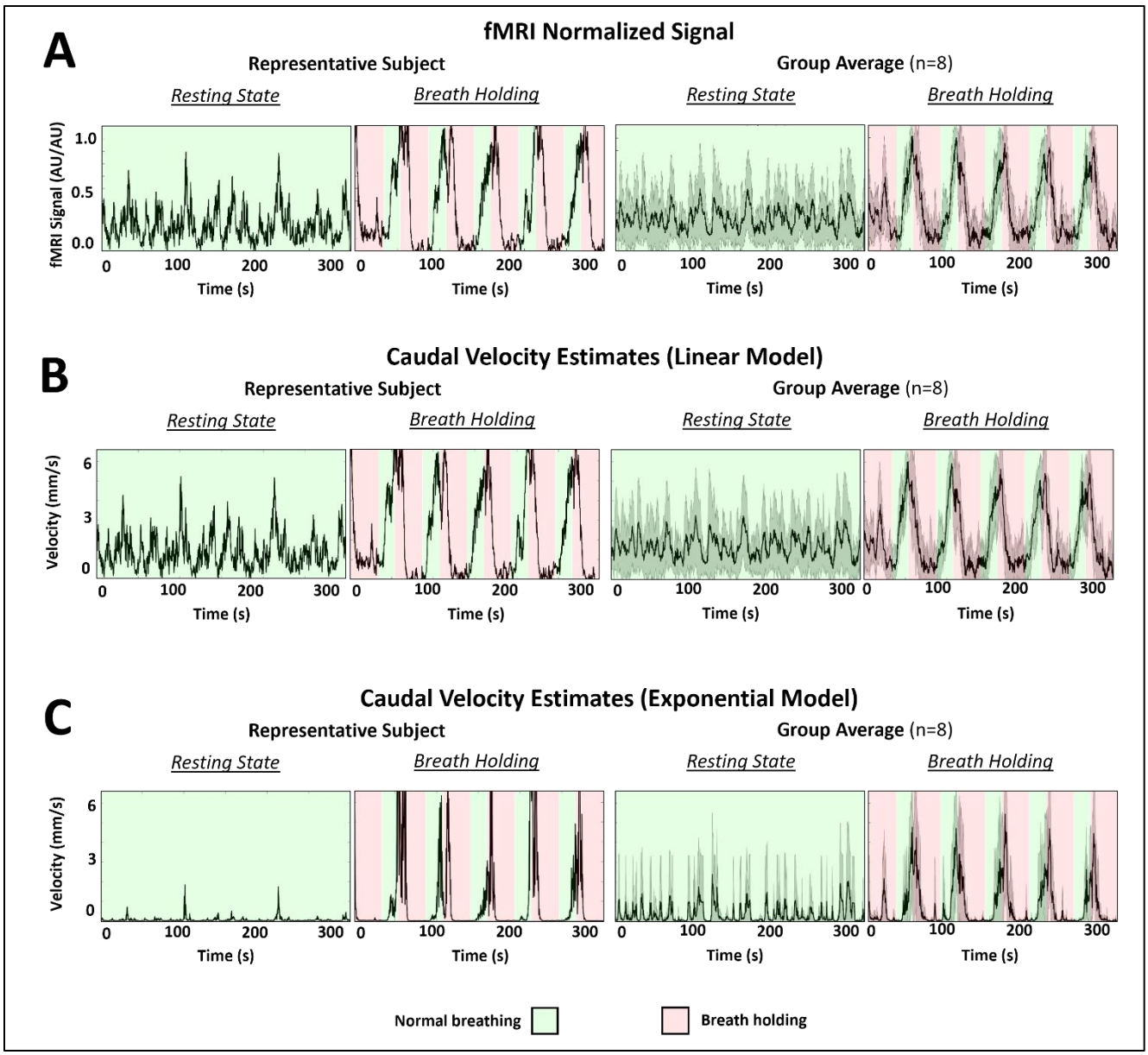

***Figure 5**: In-vivo velocity temporal waveforms in a single healthy volunteer and group average (n=8), estimated from **(A)** normalized fMRI data using **(B)** linear and **(C)** exponential fitting models. Background shading indicates Resting State free breathing (Green), where subjects were instructed to breathe normally, and Breath Holding (Red), where subjects were instructed to hold their breath.*

Discussion

CSF inflow fluctuation captured by a fast EPI sequence has been discussed in detail in Fultz et al.[4] and Yang et al.[24], but these stud[6]ies did not connect the measured inflow effect-mediated signal increases to the underlying velocities. The objective of the present study was to quantify the underlying velocities that mediate the signal increase by the inflow effect for a given set of imaging parameters relevant for *in vivo* human studies of breathing regimens. This was accomplished by performing fMRI to measure inflow effect-mediated signal increase in a controlled, experimental flow loop and using the data to fit a linear and exponential model for reconstructing velocity waveform from fMRI sequences of similar parameters. The methods developed here provide utility for approximating slow flow velocity, e.g. ventricular CSF flow, where phase-contrast methods often perform poorly due to their restriction to analyzing either slow or fast flow by a priori selection of the velocity encoding parameter.

From the data shown in **Figure 3** we observed a non-linear increase in measured fMRI signal as a function of the underlying fluid velocity. This non-linear behavior aligns with the behavior demonstrated in the 1988-2012 series of publications on quantifying signal increase by the inflow effect by Gao et al.[5–8]. Additionally,

our reconstructions of this data quantitatively demonstrated the shortcomings of a linear model and the potential for a simple two parameter exponential model to estimate underlying fluid velocity (**Figure 4**). Notably, both models fail to resolve any velocities greater than the v_{crit} since these velocities correspond to maximum volume replacement of the target voxel by unexposed fluid. Thus, the v_{crit} value is an upper limit for reconstructions utilizing this method. Our reconstruction method is best suited for slow moving fluid flow in relatively straight geometries due to the limitation of only capturing flow that is perpendicular to the imaging plane.

We tested our reconstruction methods on *in vivo* human data with the region of interest in the fourth ventricle. This location is a connection for CSF transport between the midbrain and neck, relatively straight geometry which aided in perpendicular slice placement, and has broad width which minimizes partial volume effects on the target voxels of interest. A breathing regimen that included breath holding was selected to make use of the hypercapnic response of the brain, which causes increased caudal CSF outflow due to the increased volume occupied by blood during vessel dilation. Thus, the breath holding regimen was intended to boost the underlying CSF velocity above 5.68 mm/s, which is assumed to be the critical velocity of the *in vivo* imaging sequences. It is a core assumption of this model that the fluid being measured reaches the critical velocity at some point during the series of acquisitions to ensure scaling is accomplished across the correct range.

To compare the ranges of velocities calculated by the present study, it is useful to consider recent publications that measure CSF flow with real-time phase-contrast MRI. Marcella Laganà et al. observed average CSF flow rates of 0.04 ± 0.11 ml/s for a cross-sectional area of 182.82 ± 54.34 mm^2, which equates to average CSF velocities of 0.375 ± 0.191 mm/s around the first cervical layer in the spinal canal, caudal to the fourth ventricle past the medial aperture[1]. Other studies including Baselli et al. and Yildiz et al. found caudal CSF flows of up to 2 mL/s[1] at the peridural rachis and 9.6 ± 0.7 mm/s[26] at the foramen magnum respectively, using PC-MRI. Ignoring fluid exiting via the medial aperture, these flows can be scaled via conservation of mass to the fourth ventricle cross sectional area measured via CT by Uhasai et al., who observed a fourth ventricle cross sectional area of 282.74 ± 119.24 mm² area (7.5 ± 2.5 mm anteroposterior, 12 ± 3.1 mm transverse)[14]. Using this cross-sectional area alongside the Marcella Laganà et al. and Baselli et al. flow rates, we can calculate ranges of velocities expected in the fourth ventricle to be 0.141 ± 0.781 mm/s or 7.07 ± 9.70 mm/s, respectively. Notably, these velocities vary across an order of magnitude demonstrating the variability in measurements across the field and the need for continued and alternative approaches to measuring CSF flow in real time.

The results of the present study are not intended to be generalized outside of the specific imaging parameters used within the *in vivo* and experimental studies. The increase in BOLD signal due to inflow depends on several factors, including the pulse sequence, imaging parameters, number and position of the slices, and blood T1, which is field-strength dependent[5]. The current study did not evaluate changes in these parameters, which could be used to acquire a more robust reconstruction, thus our results may only be valid for our specific combination of TR (0.44 s), z (2.5 – 2.9 mm), and flip angle (35°). Although water was used as a surrogate for CSF, it is important to note that water only approximates the solute properties and T1/T2 signal of CSF. Although the experimental data was obtained on a GE 3T scanner, the human subject data was acquired on a Siemens 3T scanner, which could introduce inters-canner variability. Despite these limitations, this method represents a novel alternative approach to estimating slow moving fluid velocities directly from fMRI with high temporal resolution and the absence of cardiac or respiratory gating requirements.

References

1. Baselli, G., F. Fasani, L. Pelizzari, M. Cazzoli, F. Baglio, and M. M. Laganà. Real-Time Phase-Contrast MRI to Monitor Cervical Blood and Cerebrospinal Fluid Flow Beat-by-Beat Variability. *Biosensors* 12:417, 2022.
2. Carotenuto, A., L. Cacciaguerra, E. Pagani, P. Preziosa, M. Filippi, and M. A. Rocca. Glymphatic system impairment in multiple sclerosis: relation with brain damage and disability. *Brain* 145:2785–2795, 2022.
3. Dreha-Kulaczewski, S., A. A. Joseph, K.-D. Merboldt, H.-C. Ludwig, J. Gärtner, and J. Frahm. Inspiration Is the Major Regulator of Human CSF Flow. *J. Neurosci.* 35:2485–2491, 2015.
4. Fultz, N. E., G. Bonmassar, K. Setsompop, R. A. Stickgold, B. R. Rosen, J. R. Polimeni, and L. D. Lewis. Coupled electrophysiological, hemodynamic, and cerebrospinal fluid oscillations in human sleep. *Science* 366:628–631, 2019.
5. Gao, J.-H. H., and H.-L. L. Liu. Inflow effects on functional MRI. *Neuroimage* 62:1035–1039, 2012.
6. Gao, J.-H., S. K. Holland, and J. C. Gore. Nuclear magnetic resonance signal from flowing nuclei in rapid imaging using gradient echoes. *Med. Phys.* 15:809–814, 1988.
7. Gao, J. H., and J. C. Gore. NMR signal from flowing nuclei in fast gradient-echo pulse sequences with refocusing. *Phys. Med. Biol.* 39:2305–2318, 1994.
8. Gao, J. H., I. Miller, S. Lai, J. Xiong, and P. T. Fox. Quantitative assessment of blood inflow effects in functional MRI signals. *Magn. Reson. Med.* 36:314–319, 1996.
9. Hillman, E. M. C. Coupling Mechanism and Significance of the BOLD Signal: A Status Report. *Annu. Rev. Neurosci.* 37:161–181, 2014.
10. Iliff, J. J. *et al.* A Paravascular Pathway Facilitates CSF Flow Through the Brain Parenchyma and the Clearance of Interstitial Solutes, Including Amyloid β. *Sci. Transl. Med.* 4:, 2012.
11. Iliff, J. J., H. Lee, M. Yu, T. Feng, J. Logan, M. Nedergaard, and H. Benveniste. Brain-wide pathway for waste clearance captured by contrast-enhanced MRI. *J. Clin. Invest.* 123:1299–1309, 2013.
12. Jenkinson, M., C. F. Beckmann, T. E. J. Behrens, M. W. Woolrich, and S. M. Smith. FSL. *Neuroimage* 62:782–790, 2012.
13. Jessen, N. A., A. S. F. Munk, I. Lundgaard, and M. Nedergaard. The Glymphatic System: A Beginner's Guide. *Neurochem. Res.* 40:2583–2599, 2015.
14. Kalathuru Uhasai, Deepti Nayak, Anil Kumar Sakalecha, Chaithanya A, Buchipudi Sandeep Reddy, Mahima Kale R, and Nallapaneni Poojitha Chowdary. Evaluation of normal measurements of fourth ventricle by computed tomography. *Asian J. Med. Sci.* 14:192–195, 2023.
15. Kollmeier, J. M., L. Gürbüz-Reiss, P. Sahoo, S. Badura, B. Ellebracht, M. Keck, J. Gärtner, H.-C. Ludwig, J. Frahm, and S. Dreha-Kulaczewski. Deep breathing couples CSF and venous flow dynamics. *Sci. Rep.* 12:2568, 2022.
16. Mokri, B. The Monro-Kellie hypothesis: Applications in CSF volume depletion. *Neurology* 56:1746–1748, 2001.
17. Tarasoff-Conway, J. M. *et al.* Clearance systems in the brain—implications for Alzheimer disease. *Nat. Rev. Neurol.* 11:457–470, 2015.
18. Vijayakrishnan Nair, V., B. R. Kish, B. Inglis, H.-C. (Shawn) Yang, A. M. Wright, Y.-C. Wu, X. Zhou, A. J. Schwichtenberg, and Y. Tong. Human CSF movement influenced by vascular low frequency oscillations and respiration. *Front. Physiol.* 13:1–14, 2022.
19. Williams, G., S. Thyagaraj, A. Fu, J. Oshinski, D. Giese, A. C. Bunck, E. Fornari, F. Santini, M. Luciano, F. Loth, and B. A. Martin. In vitro evaluation of cerebrospinal fluid velocity measurement in type I Chiari malformation: repeatability, reproducibility, and agreement using 2D phase contrast and 4D flow MRI. *Fluids Barriers CNS* 18:1–15, 2021.
20. Xie, L., H. Kang, Q. Xu, M. J. Chen, Y. Liao, M. Thiyagarajan, J. O'Donnell, D. J. Christensen, C. Nicholson, J. J. Iliff, T. Takano, R. Deane, and M. Nedergaard. Sleep Drives Metabolite Clearance from the Adult Brain. *Science (80-.).* 342:373–377, 2013.
21. Yamada, S. Cerebrospinal fluid dynamics. *Croat. Med. J.* 62:399–410, 2021.

22. Yamada, S., M. Miyazaki, H. Kanazawa, M. Higashi, Y. Morohoshi, S. Bluml, and J. G. McComb. Visualization of Cerebrospinal Fluid Movement with Spin Labeling at MR Imaging: Preliminary Results in Normal and Pathophysiologic Conditions. *Radiology* 249:644–652, 2008.
23. Yamada, S., M. Miyazaki, Y. Yamashita, C. Ouyang, M. Yui, M. Nakahashi, S. Shimizu, I. Aoki, Y. Morohoshi, and J. G. McComb. Influence of respiration on cerebrospinal fluid movement using magnetic resonance spin labeling. *Fluids Barriers CNS* 10:36, 2013.
24. Yang, H.-C. (Shawn), B. Inglis, T. M. Talavage, V. V. Nair, J. (Fiona) Yao, B. Fitzgerald, A. J. Schwichtenberg, and Y. Tong. Coupling between cerebrovascular oscillations and CSF flow fluctuations during wakefulness: An fMRI study. *J. Cereb. Blood Flow Metab.* 42:1091–1103, 2022.
25. Yavuz Ilik, S., T. Otani, S. Yamada, Y. Watanabe, and S. Wada. A subject-specific assessment of measurement errors and their correction in cerebrospinal fluid velocity maps using 4D flow MRI. *Magn. Reson. Med.* 87:2412–2423, 2022.
26. Yildiz, S., S. Thyagaraj, N. Jin, X. Zhong, S. Heidari Pahlavian, B. A. Martin, F. Loth, J. Oshinski, and K. G. Sabra. Quantifying the influence of respiration and cardiac pulsations on cerebrospinal fluid dynamics using real-time phase-contrast MRI. *J. Magn. Reson. Imaging* 46:431–439, 2017.
27. Zou, W., T. Pu, W. Feng, M. Lu, Y. Zheng, R. Du, M. Xiao, and G. Hu. Blocking meningeal lymphatic drainage aggravates Parkinson's disease-like pathology in mice overexpressing mutated α-synuclein. *Transl. Neurodegener.* 8:7, 2019.